Contrasting Target, Stray-Light, and Other Performance Metrics for MISR

Nadine C.Lu Chrien[1], Edward C. Hagerott[1], Mary L. White[1], Carol J. Bruegge[1], and Edward R. Freniere[2]
1. California Institute of Technology, Jet Propulsion Laboratory, 4800 Oak Grove Drive, Pasadena, CA 91109
2. Lambda Research Corporation 531 King Street, P.O. Box 1400, Littleton, MA 01460

The Multi-angle Imaging Spectrometer (MISR) is an Earth-observing sensor to be flown as part of the Earth Observing System (EOS) in 1998. The radiometric and spectral calibration of the nine cameras which compose this instrument will be done using targets which are uniform in space and in angle, unpolarized, and lacking in absorption lines. A calibration uncertainty will also be determined for this configuration. This allows one to estimate the accuracy of measured radiances, assuming the scene is likewise featureless with respect to these parameters. In addition to these calibrations, the MISR engineering team will be responsible for verification of certain performance specifications which assure data products can be produced for a range of target types. MISR is specified to be insensitive to the state of polarization of the incident field to within ±1%; it must recover from saturation within eight line repeat times; blooming in the event of saturation shall be limited to the eight adjacent pixels; stray-light shall be rejected to a degree sufficient to maintain the radiometric-requirements of the within-field target; and radiometry will be preserved while observing two specific contrasting scenes. The first scene is 5% in reflectance for one half-plane, and 100% in reflectance for the other half-plane. Radiance retrieval over the dark scene 24 pixels distance from the bright/ dark boundary shall differ by no more than 2% from the retrieval over a uniform 5% dark plane (lack of bright half-plane). This specification guarantees a specified level of accuracy for large dark expanse, such as the ocean surface. The second specification defines a scene which is 50% in reflectance except for the center 24x24 pixels, which are 5% in reflectance. The radiance retrieved anywhere within the dark region shall differ by no more than 2% than for the case where the scene is completely 5% dark (lacking the bright background). This scene type could be used, for example, in the aerosol retrieval algorithm where a lake surrounded by brighter land is investigated. Due to the need to estimate performance prior to hardware build, and due to the difficulties in constructing test targets for an unlimited number of scene types, MISR will be combining test and analyses to verify these specifications. Currently a stray-light analysis program is assisting in the camera design process, for the purpose of minimizing ghost imagery and spectral cross-talk. The point source transmittance function from the stray-light code is used to predict the blurring of energy in the presence of a contrasting target. Results of these analyses, and test plans will be reviewed in this presentation.

STRAY-LIGHT MODEL

In order to accurately predict stray-light in the MISR cameras, detailed stray-light models were constructed using the GUERAP V Stray-light and Radiometry Modeling Software. Models were constructed for the MISR A and D cameras, being the two extremes of four similar lens designs. These models consist of over 200 surfaces and 25 coating models. The lens barrels, retaining rings, baffles, and in particular the focal plane assembly were modeled in great detail. Each camera has a CCD detector consisting of four line arrays each with its own narrow-band, high-rejection spectral filter. The spectral passbands are centered at 443, 555, 670, and 865 nm. Diffraction was modeled at the aperture stop. Simulations were done for the 670 nm band; all coating models were constructed for properties of materials at 670 nm. The 670 nm band was chosen because it will be the most defocused, due to residual axial chromatic aberration, and diffraction concerns are minor when compared to the ghosting and geometrical aberrations. Two models were constructed for each of the A camera and D camera, one including the sunshade, and one including only the surfaces that are part of the lens and focal plane assembly. The first model was used for simulating the effects of out-of-field sources, and the second was used for in-field sources.

Description of lens

The A camera is wide angle (±14.9°) and has the shortest focal length. The D camera is narrow angle (±7.3°) and has the longest focal length. All four lens designs are telecentric and have the same F-number (5.5). Cross-sectional views of the lens designs (no focal plane assembly) are shown in Figures 1 and 2.

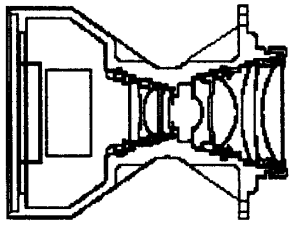

Figure 1. MISR Lens A design with barrel

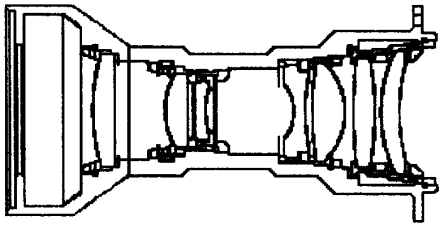

Figure 2. MISR Lens D design with barrel

Stray-light suppression measures: During the optical design phase for Lenses A, B, C, and D, the CODE V ghost image option was used to ensure that ghost images from the powered elements of the lens were minimized. The depolarizers in the front of each lens are tilted by two degrees to shift their ghosts off the CCD. All the refractive elements will be anti-reflection coated to maximize transmission while reducing ghost image effects. In addition, three knife edge black baffles were added to each lens assembly, and the retainer and positioning rings are to be black. Blackened plates with racetrack shaped apertures are attached over the depolarizer entrance aperture and another mask is located forward of the detector assembly to further reduce stray-light in each camera.

Description of focal plane assembly

There is a single design for the focal plane assembly for all cameras. The focal plane assembly contains a racetrack shaped mask, the detector window, the spectral filter which has a black mask between filter strips, and the detector. The various retainer rings and gold bond pads are also modeled.

Coating models

Anti-reflection coating specifications were used to model reflections from the lens surfaces, and the bidirectional transmittance distribution functions (BTDF) were estimated based on an assumption of 25 Å rms surface roughness using a surface-roughness bidirectional scattering distribution function (BSDF) model (Stover, 1990).

In-field stray-light

In order to assess instrument requirements for absolute radiometric accuracy, crosstalk, and detection of contrasting targets, the A and D cameras were simulated with a point source inside the field of view. The point source was focused on the 670 nm line array and on a "dead" area of the focal plane assembly adjacent to the array, at four locations (on-axis, at 40% of the field, at 80% of the field, and at full-field) along the array, i.e., in the cross-track direction. The resulting normalized irradiance distributions were converted to Point Source Transmittance (PST) for comparison with the derived PST requirements. They were also

0-7803-1497-2/94 $4.00 © 1994 IEEE

normalized to be used for convolving with specified targets to determine performance with respect to the contrasting target requirements.

Ghost image sources: Several halos of stray-light surround the focused spot, caused by two-reflection ghosts between the detector and the filter and detector window surfaces. Figures 3 and 4 show the PST distribution along the array for an on-axis point source focused on the array, for cameras A and D. The plateaus in the PST are due to ghosts, and are labeled according the surface reflections that cause the ghosts. Surface 24 is the detector and contributes to all of the strongest ghosts because of its relatively high reflectance of 0.6. Surfaces 20-23 reside in the focal plane assembly, and surfaces 16 and 17 are lens element surfaces. The sizes and intensities of the ghost images were also determined by tracing a real marginal ray using the GUERAP V program (an on-axis ray at the edge of the entrance pupil) and allowing the ray to split in two at each refracting surface. The resulting ray "tree" enumerates all the ghost images. The PST of the strongest ghost images was estimated using the formula

$$PST = \frac{\Phi_d / \left(\pi r_g^2\right)}{\Phi_i / \left(\pi r_a^2\right)} \qquad (1)$$

where Φ_d = incident flux of the ghost ray at the detector
Φ_i = incident flux of the imaging ray on the optical system
r_g = radius of the ghost image at the detector
r_a = radius of the entrance aperture.

The results of these estimates are shown in Tables 1 and 2.

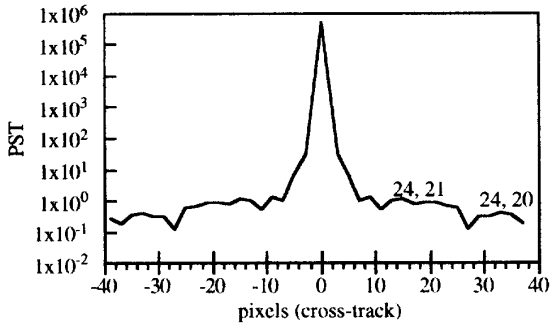

Figure 3. MISR camera A cross-section of PST.

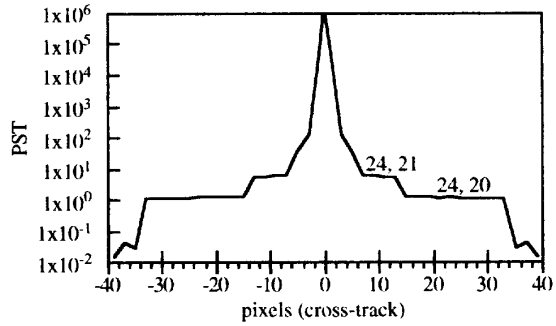

Figure 4. MISR camera D cross-section of PST.

Table 1. *MISR camera A ghost radii*

Ghost sequence	radius (pixels)	Estimated PST
24, 17	108.7	8.22E-03
24, 20	42.6	8.27E-02
24, 21	23.1	2.85E-01
24, 22	4.1	2.86E+01
24, 23	0.3	5.01E+04
24, 23, 24, 23	0.5	9.26E+02
23, 22	3.8	6.58E+00

Table 2. *MISR camera D ghost radii*

Ghost sequence	radius (pixels)	Estimated PST
24, 20	33.0	5.51E-01
24, 21	13.5	3.35E+00
24,22	4.1	1.14E+02
24, 23	0.3	1.88E+05
24, 23, 24, 23	0.4	4.04E+03
23, 22	3.8	3.35E+00
24, 16	93.2	5.61E-03

Out-of-field stray-light simulations

In order to address instrument requirements for absolute radiometric accuracy, out-of-field point sources were simulated using GUERAP V. Potential out-of-field sources of stray-light are direct sunlight and sun glints from bodies of water. The fore and aft cameras experience direct sun angles of about 30° and larger in the down-track direction only, with larger sun angles in the cross-track direction. The A nadir camera cannot receive direct sunlight. All cameras can experience sun glints from the earth near or in the field of view. For near out-of-field angles in both cameras, there are weak two-reflection ghosts with PST peaks of about 2×10^{-4}. For larger out-of-field angles, the PST is due to scattering from the depolarizers and the PST is about 1.7×10^{-9}. In the down-track direction, the depolarizers are shaded by the race-track shaped baffles beyond about 20° off-axis for both the A and D cameras. In the cross-track direction, the depolarizers are shaded beyond about 40° off-axis for the A camera and 30° for the D camera.

Cross-talk

Cross-talk in both the A and D cameras is kept low by positioning the spectral and blocking filters as close as possible to the detector array. In the simulations of images focused on the detectors, the cross-talk is negligible, and does not show up in the simulations. The PST in the down-track direction has dropped by about eight orders of magnitude at a distance five pixels from the peak. Keeping in mind that the detector arrays are spaced apart by 160 µm or about 8 pixels, we estimate that the cross-talk signal in a neighboring detector array is no more than about 10^{-9} times the peak signal. If the gap between the filter and the detector were to be increased, however, cross-talk would rapidly become a problem.

CONTRASTING TARGET MODEL

In the contrasting target model, two scene types were modeled: Scene 1, the ocean boundary, consists of two half-planes, one with 5% equivalent reflectance (ρ_{eq}), the other with 100% ρ_{eq}; Scene 2, the lake, has 50% ρ_{eq} with a 24 x 24 pixel center which has 5% ρ_{eq} (Figure 5). The results of the in-field stray-light simulations from GUERAP V were used to construct an impulse response function, sampled at 0.25 pixel intervals. This response function was then convolved with the ocean boundary scene and the lake scene to produce simulated images. These images were then rebinned (averaged) to a sampling interval of one MISR pixel. It is the simulated MISR images for camera D which are presented here.

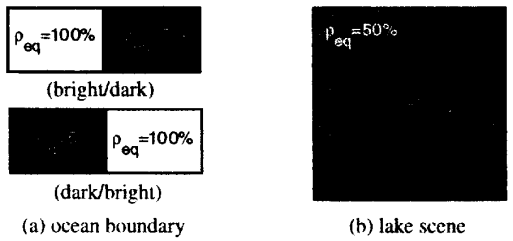

Figure 5. Contrasting targets: (a) Scene 1 and (b) Scene 2.

Scene 1 -- ocean boundary

Currently the ocean boundary has been modeled for only one orientation, the bright/dark boundary perpendicular to the length of the detector line array (cross-track direction). A cross-

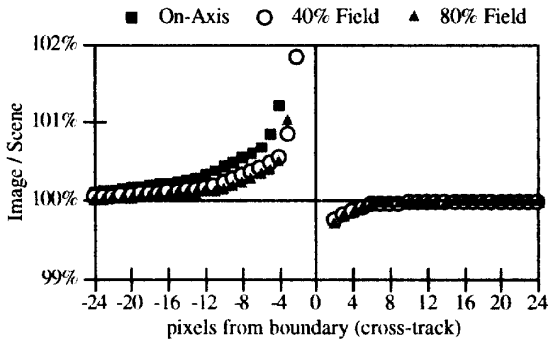

Figure 6. Normalized image of Scene 1 (Dark/Bright)

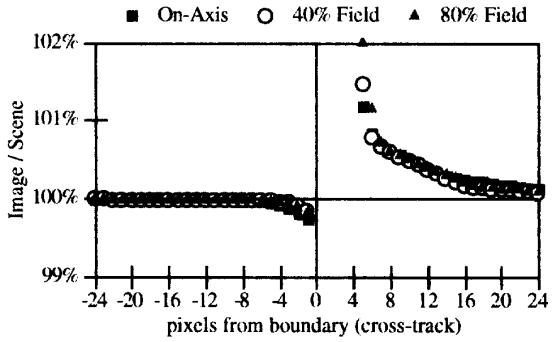

Figure 7 . Normalized image of Scene 1 (Bright/Dark).

sectional view along the line array of the resultant simulated image normalized to the input scene is shown in Figures 6 and 7. The pixel adjacent to the boundary on the dark side is approximately four times brighter than it would be in the absence of the bright plane for the bright/dark case and about two times brighter for the dark/bright case; however, at a distance of about five pixels from the boundary, the image is only about 2% brighter than an ideal image. Consequently, the pixel adjacent to the boundary on the bright side is 5% to 15% darker than it would be in the absence of the boundary.

The dark/bright image and the bright/dark image differ slightly. This is because the ghost image plateaus are not symmetric about the peak since the lens is not perfectly telecentric for all field angles. Overall the point response exhibits the same characteristic ghost plateaus with field position.

Scene 2 -- lake

The 24 x 24 pixel lake surrounded by land was also modeled. Slices through the center of the simulated image normalized to the input scene taken in the cross-track and down-track directions are illustrated in Figures 8 and 9. The vertical lines represent the bright/dark and dark/bright boundaries (or lake shores). We see that the image lake appears brighter than the scene. It is also apparent that near the boundaries the bright pixels appear slightly darker than the scene. Energy from the bright surround has strayed into the darker lake. The first pixel inside the lake boundary (i.e. the first dark pixel) can appear as much as ten times brighter than the scene. For clarity, these points were not included in the figures.

Contrasting target test plans

Four targets will be made for use in Engineering Model camera calibration. A semi-infinite field half bright and half dark, a dark 24 x 24 pixel field in a bright surround, a bright 24 x 24 pixel field in a dark surround, and a flat bright field. These targets will be projected into a camera and data will be collected at 5 positions distributed along each line array. These test targets will also be modeled and combined with the results of the stray-light model to produce simulated images for comparison with the measured results. This will provide a tie between modeled and measured results for verification of the contrasting target specifications.

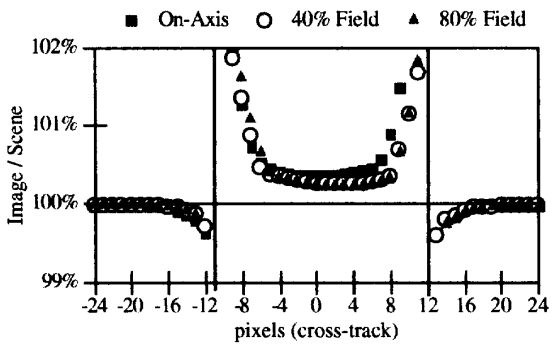

Figure 8 . Normalized image of Scene 2 (cross-track slice).

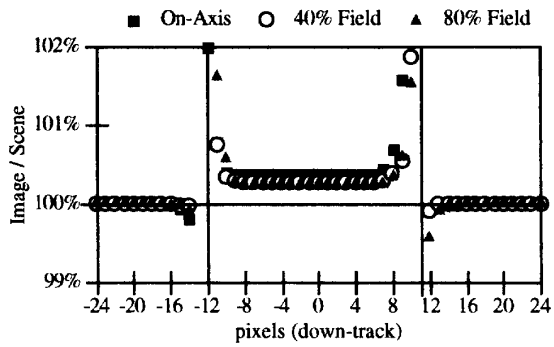

Figure 9. Normalized image of Scene 2 (down-track slice).

CONCLUSIONS

The MISR A and D cameras exhibit similar stray-light suppression performance. This is expected since the designs are very similar, being telecentric and having the same number of elements, identical detector assemblies, the same F-number, and similar baffle arrangements. From this we infer that the B and C cameras (also having similar designs and intermediate focal lengths) will have similar performance. The stray-light suppression performance is also very high, with only one significant ghost image from the lenses themselves, and all the sizable ghosts resulting from the high reflectance of the detector. The ghosts from the detector and filter surfaces might be reduced by moving these surfaces away from the detector, but cross-talk would then become a severe problem.

Through the use of optical design (CODE V) and stray-light modeling (GUERAP V) programs, the MISR cameras have been designed to minimize the effects of stray-light. Additional modeling is being utilized to predict camera performance for "real" Earth-scene targets (ocean boundary and lake). A combination of modeling and test is being used to provide an understanding of the instantaneous spatial response of the MISR cameras for particular contrasting scene types.

REFERENCES

Stover, J. *Optical Scattering: Measurement and Analysis* . New York: McGraw–Hill, 1990, pp. 83-84.

ACKNOWLEDGMENTS

The research described in this paper was carried out by the Jet Propulsion Laboratory, California Institute of Technology, under a contract with the National Aeronautics and Space Administration.